Geo-Marine Letters (2018) 38:439–455
https://doi.org/10.1007/s00367-018-0544-8

ORIGINAL

Comparing methods for computation of run-up heights of landslide-generated tsunami in the Northern Sicily continental margin

Attilio Sulli[1,2,3] · Elisabetta Zizzo[1] · Ludovico Albano[1]

Received: 9 January 2018 / Accepted: 30 July 2018 / Published online: 17 August 2018

Abstract
The North Sicily continental margin is a very active region located in the Central Mediterranean. Strong seismicity, active tectonics and volcanism, fluid escape, high sediment supply, and widespread mass movements historically have exposed this region to marine geohazards, with a potential for tsunami generation. Morpho-bathymetric analysis revealed that one of the most common mechanisms associated with marine geohazards is due to submarine mass failure processes, genetically linked to the other processes active in this margin. With the aim to assess the risks associated with landslide-generated anomalous waves, we selected two sectors of this margin, Gulf of Palermo to the west and Patti offshore to the east. The workflow included analysis of the morpho-bathymetric data, morphometric characterization, calculation of parameters of landslide-generated waves, and computation of run-ups by using different algorithms. Assuming that each of the identified landslides could be a potential tsunamigenic source, we calculated the associated theoretical run-ups, referring to the main computation methodologies proposed in the scientific literature. In order to identify the methodology that better suits run-up values for landslide-generated tsunami, we compared the known run-up values of actual, historical cases with those calculated through the different methodologies. The values obtained with the most suitable equation, both for theoretical and historical events, fit a curve that we used to formulate an empirical law describing the relationships between amplitude and depth, at the source point, and relative run-up. It can be used to calculate easily and promptly the run-up associated with a generic landslide-generated tsunami.

Introduction

Tsunamis are gravity-driven water waves, most of which generated by vertical displacement of the seabed that propagates through the water column to the surface. The resulting elevated surface wave collapses owing to gravity and then propagates outward from the source. Dispersion of the original wave generates a multiple wave train.

Tsunamis are mainly (~ 80%) generated by earthquakes, but alternative mechanisms include subaerial and submarine landslides and volcanic collapse and eruption (Tappin 2017). Their main features are represented by both the long wavelength (Charvet et al. 2013) and the height that can vary significantly from the open sea toward the coastal areas (Ezersky et al. 2013), giving the known destructive effect of tsunamis (e.g., the dramatic events in Indian Ocean 2004 and Japan 2011). Where the water depth gradually decreases, the wave slows dramatically, becomes compressed, and grows steeper. Historically known events are referred to sensational episodes which registered significant values of run-up (Ru), accompanied by the highest risks with loss of life. The study of mechanisms generating tsunami is almost exclusively focused on seismic sources because of the presence of monitoring systems widespread on the ground that allow the phenomenon to be easily attributed to a seismic event, so it is a commonplace that tsunamis are generated mostly by earthquakes.. In recent decades, morpho-bathymetric and high-resolution seismic surveys of extensive marine areas made it possible to investigate in detail the presence of large mass transport deposits, and other morphological features attributed to tectonics, volcanism, and fluid seepage.

✉ Attilio Sulli
attilio.sulli@unipa.it

[1] Dipartimento di Scienze della Terra e del Mare, Università di Palermo, Via Archirafi 22, 90123 Palermo, Italy

[2] Istituto Nazionale Geofisica e Vulcanologia, Via di Vigna Murata 605, 00143 Rome, Italy

[3] CONISMA, URL Palermo, Via Archirafi 22, 90123 Palermo, Italy

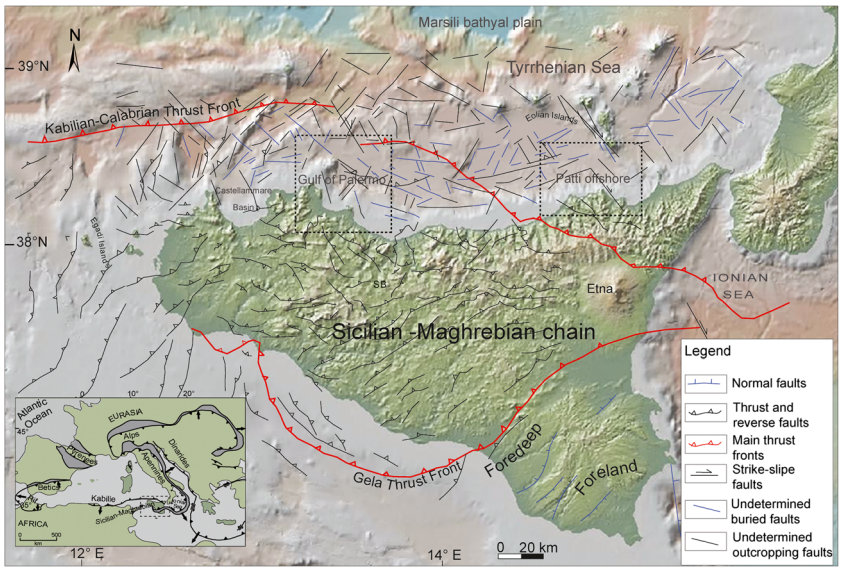

Fig. 1 Structural map of the NSCM with the main tectonic features (data from Bigi et al. 1992; Sulli 2000). In the bottom left corner, the regional setting of the central Mediterranean (from Gasparo Morticelli et al. 2015)

As a consequence, recent research has addressed tsunami sources other than earthquake, paying particular attention to landslides, which can generate large size tsunamis (Synolakis et al. 2002; Tinti et al. 2008; Liu et al. 2005; Glimsdal et al. 2013). Furthermore, medium-scale landslides (volumes lower than 1 km^3) have a higher hazard potential as they occur at higher frequency (Casalbore et al. 2011). In order to produce an adequate assessment of the potential landslide-generated tsunami (LGT), there are several statistical, graphical, and analytical methods (Harbitz et al. 2006; Enet and Grilli 2007; Dao et al. 2013; Flouri et al. 2013). Hydrodynamic simulation of landslide-generated water waves is based on laboratory experiments (Wiegel 1955; Grilli and Watts 2005; Madsen and Furman 2008), numerical modeling (Grilli and Watts 1999; Ioulalalen et al. 2006), and analytical solutions. The latter are the most common methods for LGT assessment; they are founded generally on two characterizing parameters, length and amplitude of the wave near the point source, which can be determined with algorithms based on the morphometry of submarine landslides in the neighborhood of the source area (McAdoo and Watts 2004). The main parameter of tsunamis in the coastal area is the run-up, which is a measure of the maximum vertical raising of the wave, which is a function of both the height of the incident wave to the shore, and the morphology of the coastal sector where the water mass is impacting. In most of the coastal engineering applications, practical methods are necessary to evaluate conservative estimate of tsunami parameters to be used in project calculations by operators with no experience in running detailed numerical models (Kriebel et al. 2017). Despite of some inaccuracies, simplified methods can fruitfully be used for fast tsunami hazard assessments. For mapping coastal risk, a good estimate of the maximum height reached by the wave is essential because it is closely linked to the calculation of flooding. Overall, these data are used to define a buffer zone to protect the coastal infrastructure by tsunami events. The limitations of these methods are the simplification of the phenomenon, which consider a "shallow-water," small amplitude, and long-wave model, without a detailed description of the wave shape (Didenkulova et al. 2009).

In order to verify simplified methods to assess the potential coastal and marine hazard, we analyzed the North Sicily

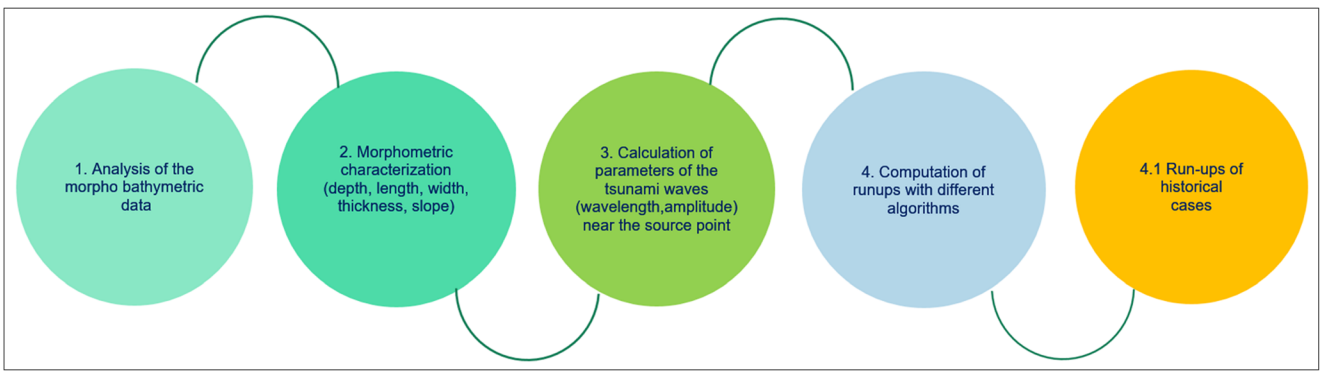

Fig. 2 The workflow used in this analysis

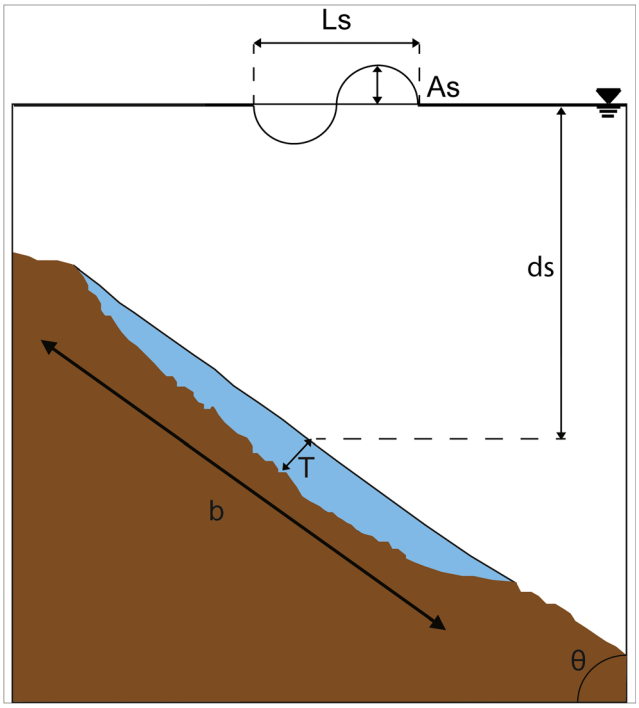

Fig. 3 Morphometric characterization of the landslide and related landslide-generated wave (for symbols, see the text)

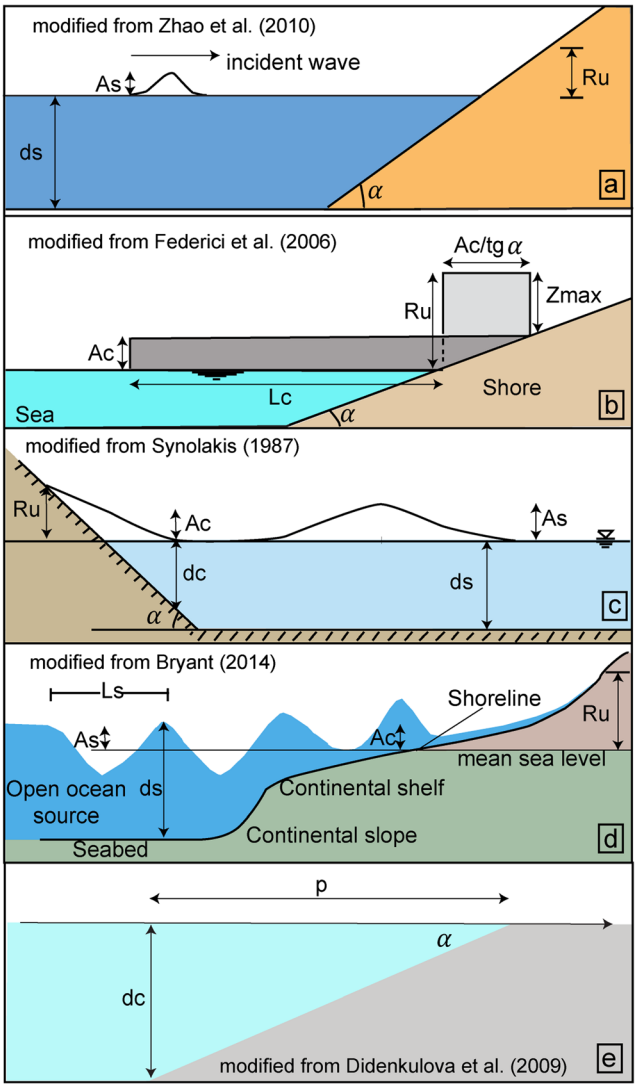

Fig. 4 Schematic models of run-up computation proposed by different authors: **a** Zhao et al. (2010), **b** Federici et al. (2006), **c** Synolakis (1987), **d** Bryant (2014), and **e** Didenkulova et al. (2009). See text for explanation of abbreviations

continental margin (NSCM), because it is a tectonically active area with potential for tsunami generation, as in the cases of Messina 1908 tsunami event (Aversa et al. 2014; Billi et al. 2010) and Stromboli 2002 tsunami event (Chiocci et al. 2008; Tinti et al. 2005; Tinti et al. 2006). Morpho-bathymetric and seismic data, recently collected in the frame of MAGIC and CARG projects, revealed the occurrence of widespread submarine mass transport, genetically related to different processes affecting this margin (canyon, fluid seepage, volcanism, tectonics). In addition, the northern Sicily is characterized by coastal mountains and hills, which are part of the Sicily fold and thrust belt, which yields a great amount of sediments that contribute to the instability of the margin. We identified two different sectors of this margin, located in the western (Gulf of Palermo) and eastern (Patti offshore) coasts, chosen based on their morphological, stratigraphic, and structural features, which could act as sources of tsunamis. Considering that most of models describing the wave propagation and calculating the tsunami parameters were proposed for open oceanic areas and they are rarely suited to semi-confined and narrow basins, the main aims of this paper are to assess the potential hazard associated with LGT in the NSCM and to identify and verify a fast analytical methodology effective for a basin with the characteristics of the Mediterranean. We selected those methods based on simple empirical relationships or obtained as results of simulations, which therefore do not require complex computations, but overall which take into account morpho-bathymetric parameters. We compared the results obtained with different methods of run-up computation applied to the potential Sicilian LGT with those related to actual events of LGT. As a result, we obtained a simple empirical formula that can be used to quickly produce inundation maps and project monitoring systems in the coastal areas exposed to tsunami hazard.

The paper follows a workflow that provides (a) the morpho-bathymetric analysis of the selected areas in the NSCM and the morphometric characterization of the main recognized landslides, (b) the calculation of the tsunami wave parameters in the source points and the computation of coastal run-ups comparing different methods, (c) the verification with historical tsunami events and selection of the best-fitting method, and (d) the formulation of an empirical law based on simple parameters, as amplitude and depth at the starting point.

Table 1 Main morphometric features of the landslides in the Gulf of Palermo

LGT	Detachment surface	Perimeter	Distance from coast	Crown depth	Coordinates	
	km^2	km	km	m	Latitude	Longitude
PMO-01	3.04	7.91	2.50	118.00	38° 08′ 28.06″ N	13° 28′ 31.08″ E
PMO-02	0.96	4.53	5.97	331.00	38° 10′ 18.36″ N	13° 28′ 45.00″ E
PMO-03	2.36	6.48	7.30	540.00	38° 11′ 04.35″ N	13° 28′ 19.71″ E
PMO-04	0.18	1.68	6.95	415.00	38° 10′ 34.17″ N	13° 27′ 56.55″ E
PMO-05	2.22	6.81	6.50	383.00	38° 10′ 47.98″ N	13° 27′ 03.27″ E
PMO-06	0.36	2.27	3.40	187.00	38° 09′ 55.10″ N	13° 24′ 58.97″ E
PMO-07	0.41	2.61	4.00	228.00	38° 10′ 31.21″ N	13° 25′ 17.65″ E
PMO-08	0.22	1.89	4.56	440.00	38° 12′ 01.50″ N	13° 25′ 03.80″ E
PMO-09	0.13	1.40	5.40	570.00	38° 12′ 31.50″ N	13° 25′ 12.89″ E
PMO-10	1.22	4.26	3.50	140.00	38° 12′ 22.97″ N	13° 24′ 10.33″ E
PMO-11	0.59	3.03	8.80	975.00	38° 13′ 52.43″ N	13° 27′ 09.10″ E
PMO-12	0.49	2.77	8.20	825.00	38° 14′ 26.59″ N	13° 26′ 05.60″ E
PMO-13	0.50	3.19	7.10	675.00	38° 14′ 22.45″ N	13° 25′ 11.57″ E
PMO-14	0.53	2.80	9.30	900.00	38° 15′ 18.46″ N	13° 26′ 01.24″ E
PMO-15	0.46	2.83	9.70	995.00	38° 15′ 25.75″ N	13° 26′ 35.72″ E
PMO-16	0.08	1.11	6.72	305.00	38° 15′ 12.85″ N	13° 23′ 18.98″ E
PMO-17	0.15	1.55	6.81	135.00	38° 15′ 49.48″ N	13° 22′ 52.91″ E
PMO-18	0.79	3.47	10.42	420.00	38° 18′ 14.50″ N	13° 23′ 26.52″ E

Geological setting

The NSCM extends in the southern Tyrrhenian Sea, from the north Sicily coastal belt to the Marsili bathyal plain (Fig. 1). The margin is located in the transitional area between the Sicilian–Maghrebian chain to the south (Agate et al. 1993) and the Tyrrhenian back-arc basin to the north (Kastens et al. 1988). This region originated as a consequence of a complex interaction of compressional events, crustal thinning, and strike-slip faulting (Trincardi and Zitellini 1987; Pepe et al. 2005). Tectonic activity started in the Miocene with the thrusting of the Kabilian-Calabrian units followed by the deformation of the Sicilian–Maghrebian chain until the early Pliocene (Sulli 2000), while the opening of the Tyrrhenian Sea led to the subsidence of the margin since the Late Tortonian (Fabbri et al. 1981). E–W, NW–SE, and NE–SW trending both extensional and compressional faults with a local strike-slip component exerted control on the morphology of the present day shelf and coastal areas during the Pleistocene.

On the continental shelf, Pleistocene deposits are truncated by an erosional surface formed during the last glacio-eustatic oscillation. Prograding sedimentary wedges of coastal deposits, formed during the Last Glacial Maximum (LGM, about 20 ka), are present along the shelf margin (Caruso et al. 2011). In the Patti sector, the occurrence of fault segments and the alternation of rocks with different competence, namely, the Hercynian metamorphic basement, its Meso-Cenozoic carbonate, Oligocene-Miocene terrigenous cover, and Pleistocene deltaic sands and gravels (Carbone et al. 1998), produced a very uneven and steep submarine morphology.

Table 2 Main morphometric features of the landslides in the Patti offshore

LGT	Detachment surface	Perimeter	Distance from coast	Crown depth	Coordinates	
	km^2	km	km	m	Latitude	Longitude
PTT-01	0.48	2.96	3.30	153.00	38° 10′ 38.82″ N	14° 42′ 07.42″ E
PTT-02	0.59	3.24	2.40	128.00	38° 11′ 16.86″ N	14° 45′ 31.06″ E
PTT-03	0.59	3.37	4.50	191.00	38° 11′ 31.84″ N	15° 00′ 50.32″ E

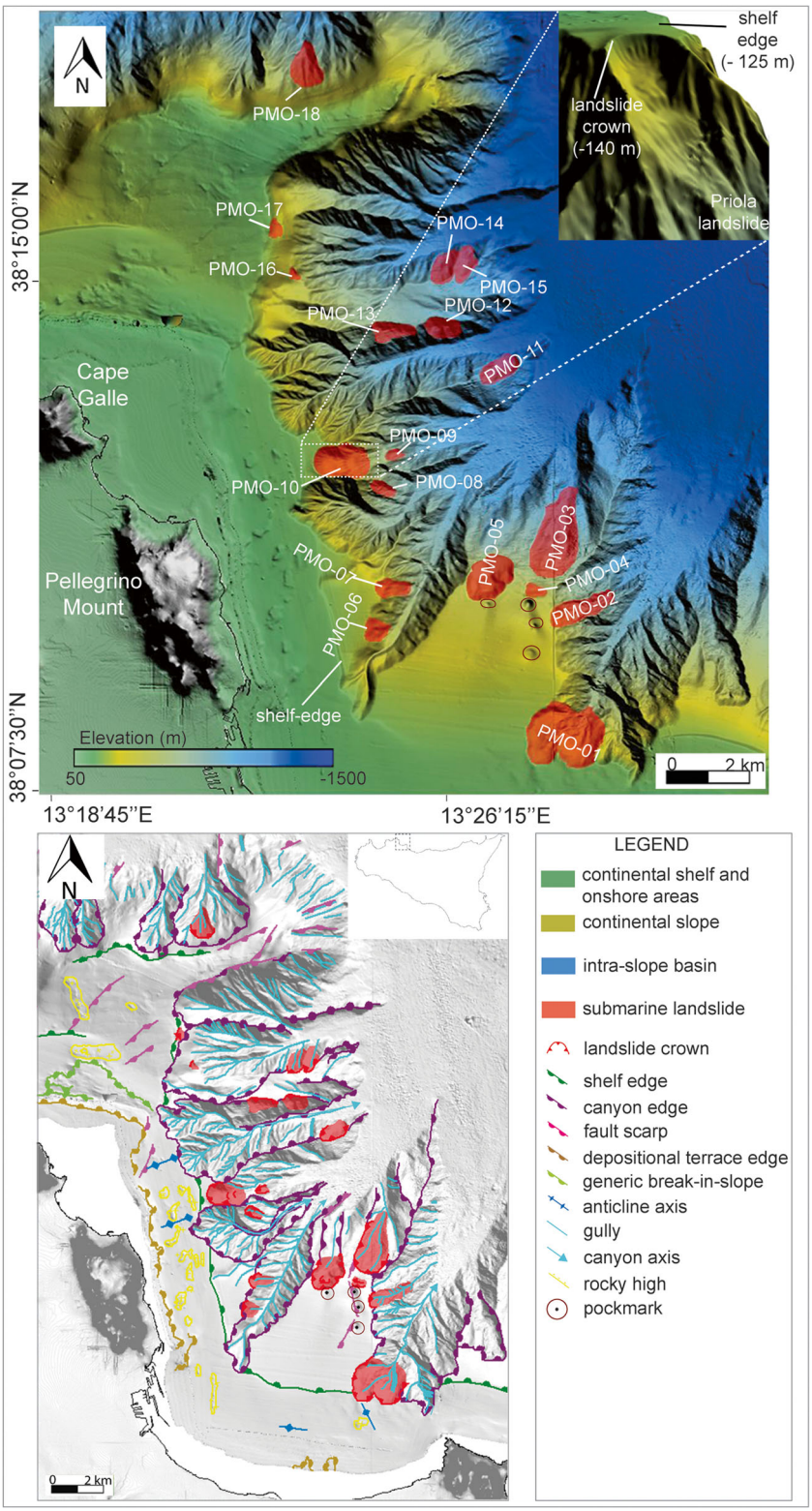

Fig. 5 Morpho-bathymetric model of the Gulf of Palermo and localization of the 18 mapped landslides. A detail of the Priola landslide (PMO-10) is shown in the top right. Canyons, gullies, and pockmarks lie in the continental slope as well as the related pockmark scars and landslides

Due to active tectonics, sedimentation, and sea-level fluctuations, both in the Gulf of Palermo (western NSCM) and the Patti offshore (eastern NSCM), swath-bathymetry shows a very active continental shelf-slope system, incised by several submarine canyons and related mass failure. The shaping of the canyons is due to both downslope evolution along tectonic

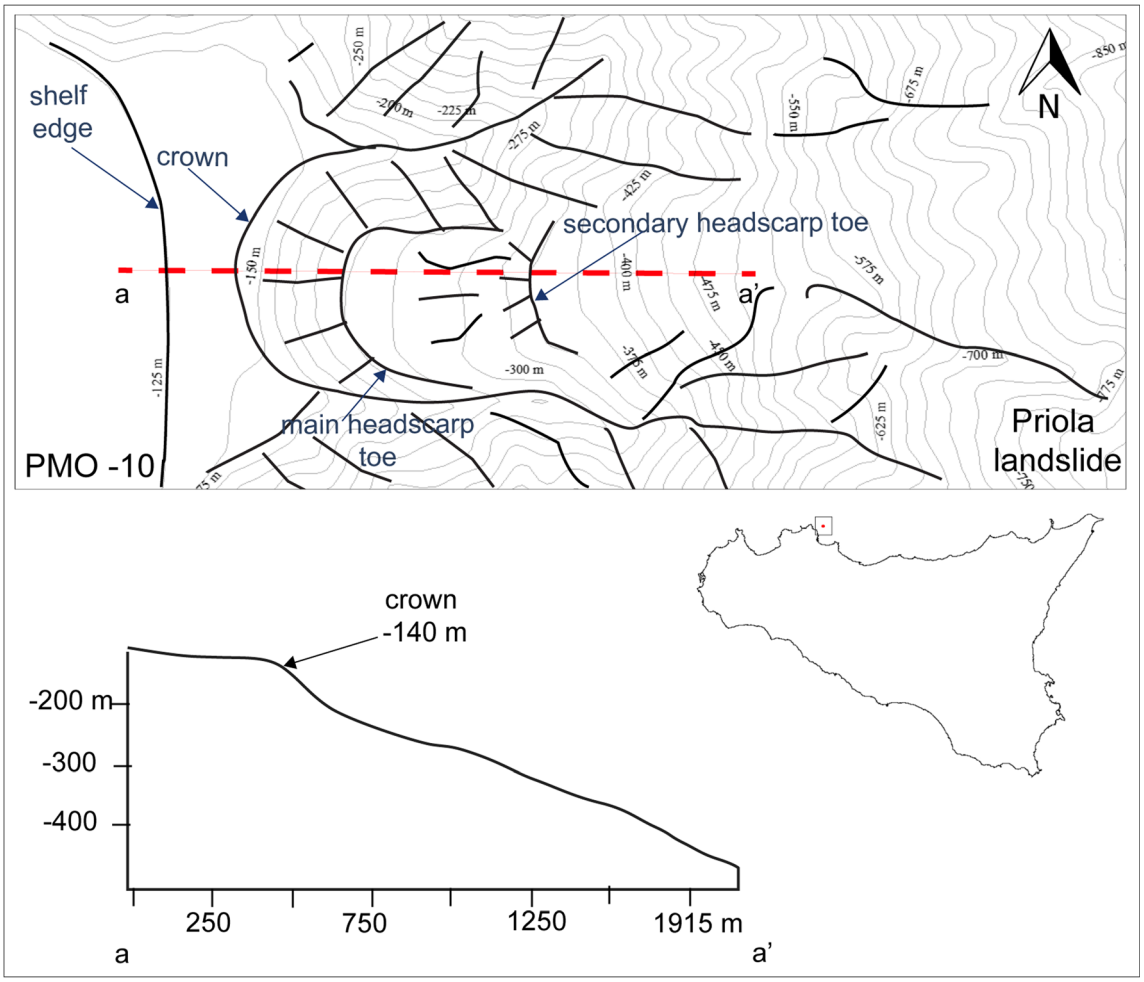

Fig. 6 Line drawing from the DTM (above) and longitudinal profile (below) of the Priola landslide (PMO-10)

lineaments, often in correspondence of the mouth of the torrential rivers, and concurrent upslope retrogressive mass failures (Lo Iacono et al. 2011; Lo Iacono et al. 2014).

The upper plate seismicity of the NSCM is defined by compressional focal mechanisms to the west and extensional to strike-slip mechanisms to the east. Shallow (< 25 km) seismic events of low to moderate magnitude (max M 5.6 in September 2002) occur along an ENE–WSW trending belt, coinciding with the Kabilian-Calabrian thrust, coupled with a NW–SE compressive offset direction (Agate et al. 2000; Giunta et al. 2009). The main seismicity of the Patti area (max M 6.1 in 1978) is linked to right-lateral NNW-SSE transcurrent systems (Neri et al. 1996).

High uplift rates during the last 125 ky were found along the eastern NSCM (0.8–1.63 mm/year) (Ferranti et al. 2010). The vertical rates show a decrease from E to W and highlight coseismic activity between adjacent sectors, while comparison between onshore and offshore sectors suggests the activity of fault systems parallel to the coastline, causing differential vertical movements (subsidence vs. uplift) (Sulli et al. 2013). The western NSCM shows a present-day stability, except for local vertical movements in the Castellammare area, where uplift rates reach 0.1–0.2 mm/year (Mauz et al. 1997; Antonioli et al. 2006).

Methods

To identify the landslides that could generate tsunamis in the NSCM, we used morpho-bathymetric data, acquired from 2001 to 2010 by the Marine GeoGroup of the University of Palermo, in the frame of CARG (national official geological cartography) and MAGIC (Marine Geohazards along the Italian Coasts) projects (oceanographic cruises DFP04, R/V Universitatis; EGUS2001, R/V Thetis; PUMA2009, R/V Universitatis; MACS2010, R/V Universitatis; Patti2003, R/V Thetis).

In the EGUS2001 and Patti2003 cruises, a Reson SeaBat 8111 MultiBeam EchoSounder (MBES), generating 105 beams with a frequency of 100 KHz and

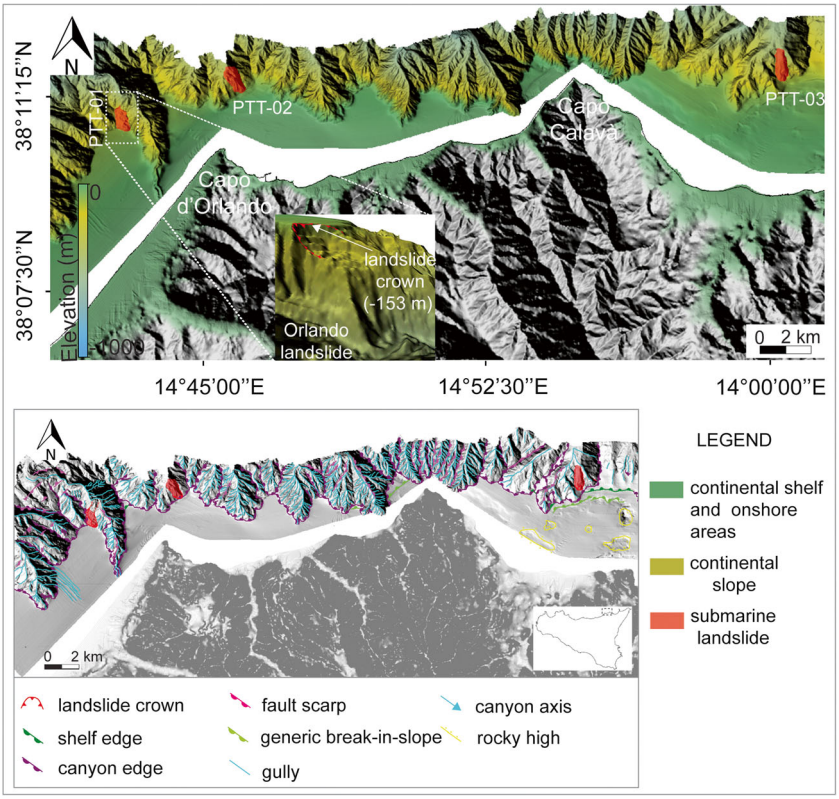

Fig. 7 Morpho-bathymetric model of the Patti offshore and localization of the three mapped landslides. A detail of the Orlando landslide (PTT-01) is shown in the inset

operational range of 20–900 m bsl, was used; in the cruises DFP04 and PUMA2009, a Reson SeaBat 8160 MBES, with a lower frequency (50 kHz), but able to investigate at higher depth (3000 m), was used. We post-processed the collected data with the software PDS2000, applying graphic removal of erroneous beams, noise filtering, processing of navigation data, and correction for sound velocity. To obtain the digital terrain model (DTM), we chose different footprint resolutions depending on the depth, with a cell size of 10 m in the shelf and 20 m in the continental slope (mean resolution of 15 m).

The workflow was developed through the following steps (Fig. 2):

1) *Analysis of the morpho-bathymetric data*. The first step was to identify and to map a large amount of submarine landslides, potentially generating tsunamis, in the Gulf of Palermo and in the Patti offshore. Golden Software Surfer and Global Mapper were used to obtain 3D maps and bathymetric profiles DTM and to analyze the morpho-bathymetric features.
2) *Morphometric characterization*. We measured the main morphometric parameters useful to calculate the potential landslide-generated anomalous wave (Fig. 3): length (b) and width (w) of landslide; its depth (ds) measured in the center point; slope angle at the source area (θ); thickness in the central point (T).
3) *Calculation of parameters of the landslide-generated wave near the source point*. Assuming each interpreted submarine landslide as tsunamigenic sources, we calculated the characterizing parameters of the landslide-generated wave near the source point, wave amplitude (As) [Eq. 1], and length (Ls) [Eq. 2] (Fig. 3), by using McAdoo and Watts (2004) equations.

$$As = 0.224\,T\left(\frac{w}{w+Ls}\right)\left[\sin\theta^{1.29} - 0.746\sin\theta^{2.29} + 0.170\sin\theta^{3.29}\right]\left(\frac{b}{ds}\right)^{1.25} \quad (1)$$

$$Ls = 3.8\left[\left(\frac{b\,ds}{\sin\theta}\right)^{0.5}\right] \quad (2)$$

Tsunamis are characterized by large wavelengths, so comparing their half-wavelengths to the ocean depths, they can be considered shallow-water waves; their amplitudes change during propagation, in agreement with the principle of energy conservation, considering that the wave speed, which is function of water depth, decreases coastward due to the fast depth decrease. The wave speed near the coast (c) can be calculated using Zhao et al. (2010) equations [Eq. 3].

$$c = \sqrt{g\,(Ac + dc)} \quad (3)$$

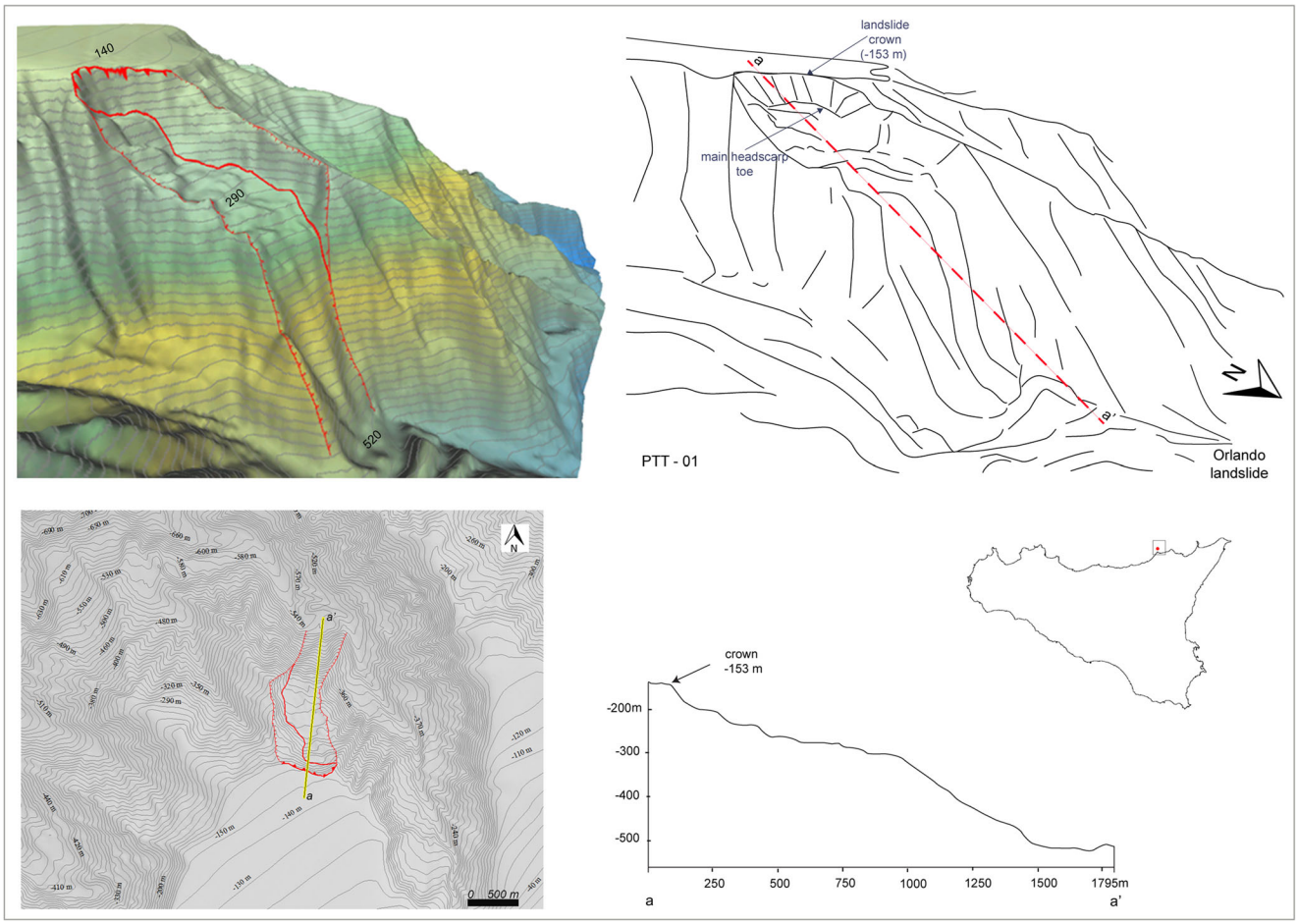

Fig. 8 Line drawing of the 3D model (above) and longitudinal profile (below) of the Orlando landslide (PTT-01)

where *dc* is the depth considered conventionally as the interference point of wave with sea bottom (10 m), *Ac* is the wave height near the coast, and *g* is the gravity acceleration. This parameter represents the shoaling process, that is, how the wave amplitude changes with the depth variation. To calculate *Ac*, we used the Green law [Eq. 4] that relates the wave amplitude at a generic point (*Ac*) to the amplitude at the source point (*As*).

$$Ac = As\left(\frac{ds}{dc}\right)^{0.25} \tag{4}$$

The obtained value of *Ac* is a rough estimate, good in correspondence of the interference point, and with the Green Law approximation, which can be accepted if we consider that wavelengths are much longer than the water depth, reducing the dispersive effects (Grilli and Watts 2005).

4) *Computation of run-ups with different simplified, approximate methods*. The run-up (Ru) is one of the main parameters that identifies the magnitude of a tsunami event. In order to estimate the tsunamigenic potential associated with submarine landslides, we calculated the Ru of waves at the coast, through different algorithms (Synolakis 1987 [Eq. 5]; Federici et al. 2006 [Eq. 6]; Didenkulova et al. 2009 [Eq. 7]; Zhao et al. 2010 [Eq. 8]; Bryant 2014 [Eq. 9]), obtained from simple empirical relationships, fluid dynamic laboratory simulations, or numerical modeling (Fig. 4), but we did not consider dispersive wave models, not consistent with a rapid computation.

In detail, Synolakis (1987) proposed an approximate theory supported by laboratory experiments and considered the run-up of solitary waves on plane beaches, describing different regimes for non-breaking or breaking waves. Federici et al. (2006) developed a GRASS-based analytical method, therefore giving emphasis to the morphological factors. Their hydrodynamic model takes into account some basic assumptions dealing with wave shape, morphology, and energy propagation. Didenkulova et al. (2009) developed an analytical method based on the solution of the non-linear shallow-water theory, but it does not take into account the wave shapes. Zhao et al. (2010) used a numerical model based on the high

Table 3 Morphometric parameters calculated for submarine mass failures in the NSCM

LGT	Length b m	Depth ds m	Slope θ °	Thickness T m	Width w m
PMO-01	1055.00	250.00	12.0	6.00	1250.00
PMO-02	800.00	500.00	18.0	10.00	750.00
PMO-03	1600.00	700.00	16.0	10.00	1000.00
PMO-04	600.00	450.00	15.0	15.00	700.00
PMO-05	1200.00	490.00	13.0	11.00	770.00
PMO-06	450.00	270.00	16.0	6.00	550.00
PMO-07	900.00	400.00	15.0	7.00	580.00
PMO-08	800.00	550.00	16.0	10.00	400.00
PMO-09	550.00	650.00	16.5	13.00	350.00
PMO-10	900.00	250.00	13.0	20.00	800.00
PMO-11	900.00	1000.00	15.0	10.00	1000.00
PMO-12	600.00	950.00	15.0	10.00	850.00
PMO-13	678.60	749.60	14.5	13.20	894.00
PMO-14	772.30	1000.00	18.0	10.00	593.00
PMO-15	500.00	1000.00	15.0	9.00	550.00
PMO-16	367.00	355.10	18.5	8.00	226.00
PMO-17	368.00	176.30	13.5	5.50	490.00
PMO-18	1300.00	667.30	18.9	15.10	933.00
PTT-01	950.00	150.00	12.0	9.00	586.00
PTT-02	1300.00	250.00	16.0	7.00	460.00
PTT-03	1380.00	260.00	15.5	6.00	480.00

order Boussinesq equations, describing analytical solution of shallow-water equations for different wave shapes. Bryant (2014) introduced a numerical model based on shallow-water long-wave equations with different morphological scenarios and different wave shapes.

Other methods (Gjevik and Pedersen 1983; Grilli et al. 1997; Gedik et al. 2005; Madsen and Fuhrman 2008) are based on similar assumptions, but are referred to peculiar conditions (type of wave, morphology, source, and so on). It is noteworthy to mention that the equations proposed by Synolakis (1987), Zhao et al. (2010), and Bryant (2014) were formulated for events generated by earthquakes.

In order to simplify the computation, the equations refer to a theoretical coastal sector, where the height of the waves does not change with the morphology of the coast and during the propagation of the wave, the energy does not decrease.

$$Ru = dc\ 2.831\left(\sqrt{\cot\alpha}\right)\left(\frac{Ac}{dc}\right)^{5/4} \tag{5}$$

$$Ru = Ac + \sqrt{\frac{c^2}{2g}\tan\alpha\left(Lc + \frac{Ac}{2\tan\alpha}\right)} \tag{6}$$

$$Ru = 3.5\ Ac\sqrt{\frac{p}{Lc}} \tag{7}$$

$$Ru = 3.043\ Ac\sqrt{c\sqrt{\frac{3Ac}{4\ dc^3}}\left(\frac{dc\cot\alpha}{\sqrt{g\ dc}}\right)} \tag{8}$$

$$Ru = 2.83\ \sqrt{\cot\alpha}\ Ac^{5/4} \tag{9}$$

To apply these algorithms, we had to calculate other parameters:

α—slope of the coastal strip (we assumed it equal to 1°, considering the investigated regions);
p—Breaking point–coastline interval (considering a breaking point depth of 10 m and a constant slope of 1°, it geometrically corresponds to a constant value of 588.23 m).
k—wave number (according to Zhao et al. 2010) [Eq. 10]

$$k = \sqrt{\frac{3Ac}{4\ dc^3}} \tag{10}$$

Table 4 Wavelength and amplitude values at the source point

LGT	Wavelength Ls m	Wave amplitude As m
PMO-01	4358.81	0.20
PMO-02	4403.01	0.10
PMO-03	7801.01	0.11
PMO-04	3952.71	0.10
PMO-05	6256.85	0.10
PMO-06	2569.39	0.07
PMO-07	4564.19	0.07
PMO-08	4889.54	0.04
PMO-09	4341.88	0.03
PMO-10	3870.42	0.47
PMO-11	7216.62	0.03
PMO-12	5743.15	0.02
PMO-13	5516.11	0.05
PMO-14	6118.05	0.02
PMO-15	5378.95	0.01
PMO-16	2480.17	0.03
PMO-17	2040.18	0.08
PMO-18	6333.24	0.18
PTT-01	3203.90	0.35
PTT-02	4202.27	0.19
PTT-03	4484.23	0.16

Table 5 Basic parameters useful for the calculation of the run-up. The calculations were carried out considering a theoretical coastal sector characterized by a slope of 1° (average value of inner continental shelf) and by a depth of interference with the seafloor of 10 m

LGT	Slope α °	Wave amplitude Ac m	Wavelength Lc m	Speed c m/s	Depth dc m
PMO-01	1.0	0.46	261.41	10.13	10.00
PMO-02	1.0	0.27	339.76	10.04	10.00
PMO-03	1.0	0.32	313.33	10.06	10.00
PMO-04	1.0	0.27	340.39	10.03	10.00
PMO-05	1.0	0.27	340.33	10.03	10.00
PMO-06	1.0	0.16	445.62	9.98	10.00
PMO-07	1.0	0.18	421.19	9.99	10.00
PMO-08	1.0	0.11	525.04	9.96	10.00
PMO-09	1.0	0.08	626.96	9.94	10.00
PMO-10	1.0	1.04	172.60	10.41	10.00
PMO-11	1.0	0.11	536.29	9.96	10.00
PMO-12	1.0	0.07	654.34	9.94	10.00
PMO-13	1.0	0.15	458.56	9.98	10.00
PMO-14	1.0	0.08	630.41	9.94	10.00
PMO-15	1.0	0.04	934.94	9.92	10.00
PMO-16	1.0	0.07	678.45	9.94	10.00
PMO-17	1.0	0.16	445.36	9.98	10.00
PMO-18	1.0	0.52	245.05	10.16	10.00
PTT-01	1.0	0.69	211.93	10.24	10.00
PTT-02	1.0	0.42	273.45	10.11	10.00
PTT-03	1.0	0.35	298.02	10.07	10.00

Lc—wavelength near the coastal sector (according to Federici et al. 2006*)* [Eq. 11]

$$Lc = \frac{4\,q\,dc}{\sqrt{3\frac{Ac}{dc}}} \tag{11}$$

4.1) *Computation of run-ups with different equations: run-ups of historical cases*. The considered equations were applied to actual historical cases. We considered historical cases of LGT, extending worldwide because Mediterranean tsunamis are almost completely attributed to earthquakes. We selected LGT with more detailed information, to apply the described equations and to

Table 6 Computed run-ups, obtained by using five methods proposed by different authors

LGT	Ru Synolakis (1987) m	Ru Federici et al. (2006) m	Ru Didenkulova et al. (2009) m	Ru Zhao et al. (2010) m	Ru Bryant (2014) m
PMO-01	4.51	5.46	2.39	4.56	14.46
PMO-02	2.34	5.85	1.24	2.36	11.12
PMO-03	2.86	5.70	1.52	2.89	12.06
PMO-04	2.33	5.85	1.24	2.34	11.10
PMO-05	2.33	5.85	1.24	2.35	11.10
PMO-06	1.19	6.47	0.63	1.19	8.48
PMO-07	1.37	6.33	0.73	1.37	8.97
PMO-08	0.79	6.94	0.42	0.79	7.20
PMO-09	0.51	7.52	0.27	0.51	6.03
PMO-10	12.72	5.46	6.75	13.04	21.90
PMO-11	0.75	7.01	0.40	0.75	7.05
PMO-12	0.45	7.67	0.24	0.46	5.78
PMO-13	1.11	6.55	0.59	1.11	8.24
PMO-14	0.50	7.54	0.26	0.50	5.99
PMO-15	0.19	9.09	0.10	0.19	4.04
PMO-16	0.42	7.80	0.22	0.42	5.57
PMO-17	1.19	6.47	0.63	1.19	8.49
PMO-18	5.30	5.40	2.81	5.36	15.42
PTT- 01	7.61	5.34	4.04	7.74	17.83
PTT- 02	4.03	5.51	2.14	4.07	13.82
PTT- 03	3.25	5.63	1.72	3.28	12.68

Table 7 Morphometric parameters of the submarine mass failures responsible for historical events

LGT case history	Length b m	Depth ds m	Slope θ °	Thickness T m	Width w m
Mona Passage (1918)	8500.00	1900.00	9.0	100.00	8500.00
Valdez (1964)	450.00	150.00	2.0	10.00	1300.00
Nice (1979)	4000.00	450.00	6.0	25.00	4800.00
Papua (1998)	4000.00	1100.00	5.0	600.00	4100.00

compare computed theoretical results with real values, to identify the equation that provides the most reliable results. Morphometric parameters were extrapolated from available data or integrated with low-resolution morpho-bathymetric data available online (http://www.gebco.net).

Following the selection of the best method to calculate the LGT run-ups, we put together actual LGT and potential Palermo Gulf and Patti offshore LGT and found the relative best-fitting curve to extrapolate a fast empiric equation that allows calculating quickly run-ups.

Results

Throughout the study areas, we identified and parameterized, but not classified, 21 significant landslides, 18 in the Gulf of Palermo (Table 1) and 3 in the Patti offshore (Table 2) respectively, on the basis of bathymetric and morphological features, such as size, depth, and distance from the coast (Figs. 5 and 7).

The submarine mass failures in the NSCM. The Gulf of Palermo

The continental shelf in the Gulf of Palermo occupies an area of approximately 250 km^2 and is 8 km wide on average. The Gulf of Palermo shows a very active continental shelf-slope system, incised by several submarine canyons, which locally indent the shelf-edge and flow into the Palermo intraslope basin, at a depth of around 1300 m. Most of the mass failures of the area are related to canyon shaping processes, and only few of them are not confined to the upper slope (Fig. 5). The continental shelf is characterized by mounds and pockmarks. The average height of the mounds is approximately 80 m, and their maximum area is about 50,000 m^2, while the average depth of pockmarks is about 20 m and the maximum area is 85,000 m^2 (Fig. 5). The canyons evolved through concurrent top-down turbiditic processes and bottom-up retrogressive mass failures, whose average length is about 5000 m, while the mean width is about 1000 m The main geological feature that controls the evolution of the canyons and induces sediment instability is the steep (1–10°) slope gradient. Faults and antiforms contributed to the regulation of mass failure processes, while the alignment of pockmarks and authigenic carbonates suggests a relationship between structural control, fluid escape processes, and mass failures (Lo Iacono et al. 2011).

The 18 main submarine landslides of the Palermo Gulf (Fig. 5), observed along the upper slope, are presented from the east to the west in Table 1. The main mass failure is the well-preserved Priola landslide (PMO-10), affecting the uppermost slope, at a depth of 150 m. The scar (Fig. 6), which is about 900 m wide and 100 m high, displays a semicircular shape and a failure plan flattening toward the detachment area, indicating a rotational component in a general translational mass movement. A detailed description of the morphometric characters of the landslides is presented in Table 1.

The submarine mass failures in the NSCM. The Patti offshore

In the Patti offshore, the shelf margin is strongly uneven and mainly located at a depth of 140–145 m (Fig. 7). A dense network of canyons, gullies, channel-levee systems, structural

Table 8 Wave parameters near the source point for historical events

LGT case history	Wavelength Ls m	Wave amplitude As m
Mona Passage (1918)	39,321.58	2.09
Valdez (1964)	5382.12	0.02
Nice (1979)	16,059.42	0.99
Papua (1998)	27,497.25	3.52

Table 9 Wave parameters near the coast for historical events. We considered a theoretical slope of 1° in the coastal sector

LGT case history	Slope α °	Wavelength Lc m	Wave amplitude Ac m
Mona Passage (1918)	1.0	63.16	7.80
Valdez (1964)	1.0	845.53	0.04
Nice (1979)	1.0	110.02	2.57
Papua (1998)	1.0	52.22	11.41

Table 10 Theoretical values of run-ups for historical events obtained with the different methodologies. The last column shows their actual run-up values

LGT case history	Theoretical values					Actual values
	Ru Synolakis (1987) m	Ru Federici et al. (2006) m	Ru Didenkulova et al. (2009) m	Ru Zhao et al. (2010) m	Ru Bryant (2014) m	Ru m
Mona Passage (1918)	156.98	14.47	83.26	181.37	59.83	6.00
Valdez (1964)	0.24	8.66	0.13	0.24	4.47	6.00
Nice (1979)	39.21	7.06	20.80	41.53	34.35	3.50
Papua (1998)	252.55	19.82	133.97	305.57	72.37	12.50

steps and highs, submarine terraces and landslides, and sedimentary creep features shows that the margin is very young and continuously reactivated by tectonic processes.

The shaping of the canyons is due to both downslope evolution along tectonic lineaments, often in correspondence of the mouth of torrential rivers, and concurrent upslope retrogressive mass failures. The landslides analyzed in the Patti offshore are presented in Table 2.

The well-preserved Orlando landslide (PTT-01 in Table 2) is located in the upper slope, at a minimum depth of 153 m. The scar (Fig. 8), which is about 586 m wide and has a detachment surface of 0.48 km^2 and a perimeter of 2.96 km, shows a semicircular shape and a plane flattening to the detachment zone, which indicates a rotational component in a translation mass movement. It is only 3.3 km far from the coast.

Landslide morphometry and run-up computation

With the aim to compute the expected run-up for theoretical LGT, we measured the morphometric parameters of each landslide (Table 3), considering them as potential source of tsunami waves. The morphometric analysis confirms that the Priola (PMO-10) landslide is the main feature in the Palermo Gulf, while the Orlando (PTT-01) landslide is the most prominent feature in the Patti offshore.

The *As* and *Ls* values were calculated to model the hypothetical wave generated near the source point from the identified submarine landslides, by using the McAdoo and Watts (2004) equations (Table 4).

Starting from these values, we calculated the basic parameters to compute the expected run-ups for each landslide (Table 5). In Table 5, we can notice that the maximum wave

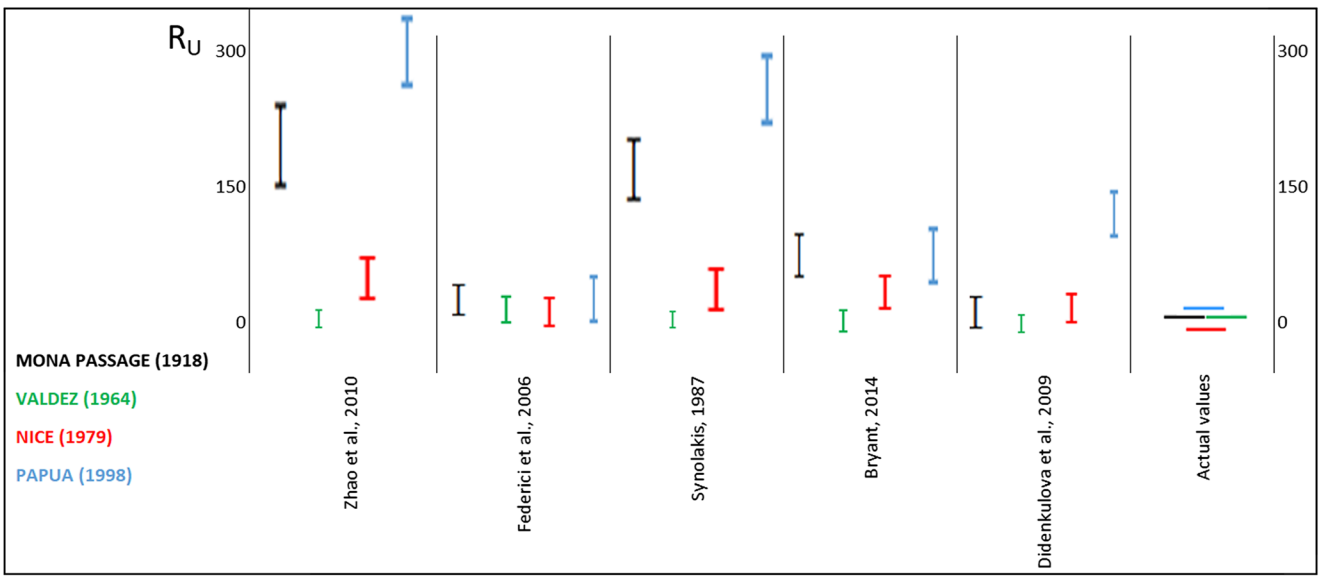

Fig. 9 Comparison between Ru values (in meters) obtained with the different methods (with error bars) and the observed values of historical events (error bars not assessable)

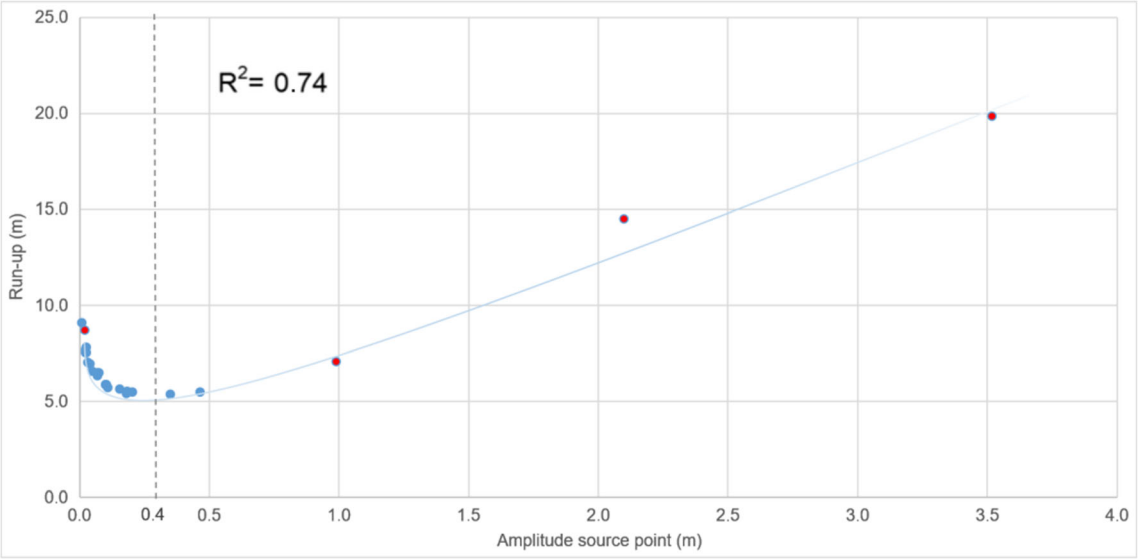

Fig. 10 Relationship between the wave amplitude near the source point and computed run-ups of NSCM (blue dots) and actual (red dots) LGT. The occurrence of a critical amplitude value is outlined at 0.4 m. The R^2 is higher than 0.7, pointing out a good fitting between values and curve

amplitude near the coast is 1.04 m (PMO-10), and the minimum value is 0.04 m (PMO-15); the maximum wavelength near the coast is related to PMO-15, and the minimum value is for PMO-10.

Subsequently, we computed the values of run-ups referred to the interpreted submarine landslides (Table 6). By applying the different equations, the run-up values change strongly for the analyzed landslides. In particular, from the comparison of the different methods used in both sectors (Gulf of Palermo and Patti offshore), characterized by different geological and morphological parameters, we found that the obtained Ru values are very different. In detail, the higher values of Ru are those obtained with the Bryant (2014) method (with maximum values of 21.9 and 17.83 m related to PMO-10 and PTT-O1 for Palermo and Patti respectively), while the lower values are those calculated with Didenkulova et al. (2009). From our results, it is also evident that there are no appreciable differences among the run-up values obtained with the methods proposed by Zhao et al. (2010) and Synolakis (1987), while the Federici et al. (2006) method provides Ru values included in a short interval between 5.34 and 9.09 m (Table 6).

Discussion

In general, the results show that most of the submarine landslides are confined on canyon walls. As a consequence, they could propagate without significant loss of energy, representing therefore a significant hazard and a threat of tsunamis along the coast. Moreover, these landslides could be element of potential risk also for underwater installations or cables.

But the comparison among swift methods used to assess run-ups related to both landslide- and earthquake-generated tsunamis showed that the values calculated with different equations can differ very much. In order to identify the best method to obtain the most realistic value of LGT run-ups, we tested all the algorithms with historical events, in order to verify the values obtained with different equations with actual values. To do this, we selected historical events of LGT where we found thorough data sufficient to get the parameters that we have to enter into the equations. In particular, we analyzed four cases of LGT:

- *Mona Passage* (between Hispaniola and Puerto Rico), occurred on October 11, 1918 (López-Venegas et al. 2008)
- *Valdez* (Alaska), where on March 27, 1964, a strong earthquake triggered a large submarine landslide that generated a tsunami, with run-ups of 6 m (Parsons et al. 2014; Nicolsky et al. 2010)
- *Nice* (France), occurred on October 16, 1979 (Labbé et al. 2012)
- *Papua* (New Guinea) occurred on July 17, 1998 (Tappin et al. 2008; Heinrich et al. 2000)

For these events, we calculated the morphometric parameters that are reported in Table 7.

Subsequently, we calculated the parameters relative to the height and length of the tsunami wave near the source point (Table 8) and near the coast (Table 9).

Based on these parameters, we computed with the different equations the theoretical values of run-up (Table 10) and compared the results with the actual values. The comparison showed that with the methods proposed by Zhao et al. (2010), Synolakis (1987), and Bryant (2014), for events

Table 11 Spread (Δ) between the results obtained with the empirical equation compared to those obtained from Federici et al. (2006), both in relation to the values of actual LGT

LGT	Ru Federici et al. (2006)	Ru our equation	Δ Ru Federici et al. (2006)–Ru our equation
	m	m	m
PMO-01	5.46	5.98	−0.52
PMO-02	5.85	6.04	−0.19
PMO-03	5.70	6.01	−0.31
PMO-04	5.85	6.03	−0.18
PMO-05	5.85	6.04	−0.19
PMO-06	6.47	6.30	0.18
PMO-07	6.33	6.28	0.04
PMO-08	6.94	6.93	0.01
PMO-09	7.52	7.77	−0.26
PMO-10	5.46	6.56	−1.10
PMO-11	7.01	7.30	−0.29
PMO-12	7.67	8.29	−0.62
PMO-13	6.55	6.64	−0.09
PMO-14	7.54	8.10	−0.57
PMO-15	9.09	11.70	−2.61
PMO-16	7.80	7.79	0.01
PMO-17	6.47	6.21	0.26
PMO-18	5.40	5.96	−0.56
PTT-01	5.34	6.27	−0.93
PTT-02	5.51	5.96	−0.45
PTT-03	5.63	5.95	−0.32
Mona Passage (1918)	14.47	11.34	3.13
Valdez (1964)	8.66	8.46	0.20
Nice (1979)	7.06	8.05	−0.99
Papua (1998)	19.82	15.59	4.23
LGT	Ru actual values	Ru our equation	Δ Ru actual values–Ru our equation
	m	m	m
Mona Passage (1918)	6.00	11.34	−5.34
Valdez (1964)	6.00	8.46	−2.46
Nice (1979)	3.50	8.05	−4.55
Papua (1998)	12.50	15.59	−3.09

generated by earthquakes, as well as those coming from the Didenkulova et al. (2009) algorithm, we obtained theoretical values diverging very much from the actual values of run-ups, even more than 290 m higher (Papua Ru calculated with the Zhao et al. (2010) method) and more than 5.80 m lower (Valdez Ru calculated with the Didenkulova et al. (2009) equation). Differently, the method proposed by Federici et al. (2006) returns theoretical values comparable with the actual run-ups for all the considered events (Fig. 9). We motivate this result considering that this method takes into account the wave parameters (wavelength and speed) in the coastal sector, as well as morphological features (slope), so their model describes better the environmental conditions near the shore. While Zhao et al. (2010) do not consider slope and wavelength, Synolakis (1987) and Bryant (2014) equations do not include wavelength and speed, and Didenkulova et al. (2009) ignore slope and wave speed. Really, we have to consider however that Federici et al. (2006) developed their model in semi-confined and narrow basins (Mediterranean and Caribbean seas), similar to those of the considered historical events (lagoons, embayments, or restricted basins). Besides, this method does not consider increase in wave height in restricted areas and loss of energy during propagation and assumes that the wavefront is parallel to the coast.

The results coming from the equation of Federici et al. (2006) are always higher than the measured ones. This is a very important aspect because it represents a precautionary element for the assessment of the geological hazard of LGT.

For this reason, we took into account the values returned by this algorithm to draw a graph in order to relate the expected

run-up values (relative to both the NSCM and actual LGT events), according to Federici et al. (2006), to the wave amplitude near the source point (Fig. 10).

Analyzing the resulting graph, it is clear that the distribution is ordered according to a curve where the highest values of run-ups are in direct proportionality, as expected, with the wave amplitude.

Nevertheless, a small section of the curve shows an opposite trend: for very low wave amplitude (< 0.4 m) values, an increase in run-up values is observed with decreasing amplitudes. It means that for amplitudes higher than 0.4 m, the greater contribution is given by the value of the amplitude, while for values less than 0.4 m, the major contribution to the run-up does not derive from the value of the wave amplitude at the source point. If we consider the second term of Eq. 7, which represents the maximum raising reached by the water respect to the wave amplitude (Zmax in Fig. 4b), the major contribution could be related to c (wave speed near the coast) and/or Lc (wavelength near the coast).

Based on the drawn curve, we deduced an empirical equation [Eq. 12] linking the wave amplitude to the expected run-ups and fitting the plotted values:

$$Ru = \frac{3As^2 + 5As + 0.075}{As} \quad (12)$$

This equation has been applied both to the hypothetical LGT events in the NSCM studied areas and to the historical actual events. The results (Table 11), compared to the run-up values of the actual events, are surprisingly more fitting than those obtained from Federici et al. (2006), even if the differences are minimal. In this way, we propose an empirical method of tsunami computation that, notwithstanding the lack of theoretical backing, allows obtaining very promptly run-up values of LGT, which can be used in rapid assessment or to draw flooding maps in large regions.

But end-users of this simplified approach must consider that it is an approximate method that takes into account only parameters of the source point, and not morphological features of the coastal areas, and overall that we tested it for LGT and not for earthquake-generated tsunamis. Furthermore, the values of run-up obtained from the curve are overestimated, representing precautionary conditions for the assessment of the geological hazard.

Conclusions

Analyzing the morpho-bathymetry data of the northern Sicily continental margin, a tectonically active sector of the central Mediterranean characterized by widespread instability, several submarine landslides were identified.

Assuming that each of them could be a potential tsunamigenic source, we calculated the associated theoretical run-ups, comparing approximation methods proposed in the literature.

In order to identify the methodology that better suits LGT values, we compared the known run-up values of actual cases with those calculated through the different methodologies. Once verified that the Federici et al. (2006) method better approximates the values of actual LGT events, we formulated an empirical law that allows calculating promptly the run-up associated with a generic LGT having as starting data the amplitude of the wave near the source point.

Acknowledgements We are very grateful to the Editor, Karin Bryan, and the anonymous reviewers for the constructive suggestions that improved significantly the manuscript.

Funding information Funding for research was provided by CARG and MAGIC projects (CONISMA/URL Palermo) and MIUR/University of Palermo (PJ_AUTF_008539) (resp. A. Sulli).

References

Agate M, Beranzoli L, Braun T, Catalano R, Favali P, Frugoni F, Pepe F, Smriglio G, Sulli A (2000) The 1998 offshore NW Sicily earthquakes in the tectonic framework of the southern border of the Tyrrhenian Sea. Mem Soc Geol It. 55:103–114

Agate M, Catalano R, Infuso S, Lucido M, Mirabile L, Sulli A (1993) Structural evolution of the Northern Sicily continental margin during the Plio-Pleistocene. In: Max, M.D., Colantoni, P. (Eds.), Geological development of the Sicilian–Tunisian platform. UNESCO Report In Marine Science 58: 25–30

Antonioli F, Kershaw S, Renda P, Rust D, Belluomini G, Cerasoli M, Radtke U, Silenzi S (2006) Elevation of the last interglacial highstand in Sicily (Italy): a benchmark of coastal tectonics. Quaternary International 145-146:3–18

Aversa M, Bussoletti G, Fea M, Torre R (2014) I maremoti nell'area dello Stretto di Messina - the seaquakes in the Messina Strait area. Mem. Descr. Carta Geol. d'It XCVI:87–128

Bigi G, Bonardini G, Catalano R, Cosentino D, Lentini F, Parotto M, Sartori R, Scandone P, Turco E (1992) Structural model of Italy, 1: 500.000. Consiglio Nazionale delle Ricerche, Rome

Billi A, Minelli L, Orecchio B, Presti D (2010) Constraints to the cause of three historical tsunamis (1908, 1783, and 1693) in the Messina Straits Region, Sicily, Southern Italy. Seismological Research Letters 81(6):907–915. https://doi.org/10.1785/gssrl.81.6.907

Bryant E A (2014) Tsunami, the underrated hazard. Springer International Publishing Switzerland p. 222. doi: https://doi.org/10.1007/978-3-319-06133-7_2

Carbone S, Lentini F, Vinci G (1998) Carta geologica del settore occidentale dei Monti Peloritani (Sicilia nord-orientale). S.EL.CA., Firenze

Caruso A, Cosentino C, Pierre C, Sulli A (2011) Sea-level changes during the last 41,000 years in the outer shelf of the southern Tyrrhenian Sea: evidence from benthic foraminifera and seismostratigraphic analysis. Quaternary International 232:122–131. https://doi.org/10.1016/j.quaint.2010.07.034

Casalbore D, Romagnoli C, Bosman A, Chiocci FL (2011) Potential tsunamigenic landslides at Stromboli Volcano (Italy): insight from

marine DEM analysis. Geomorphology 126:42–50. https://doi.org/10.1016/j.geomorph.2010.10.026

Charvet I, Eames I, Rossetto T (2013) New tsunami runup relationships based on long wave experiments. Ocean Modelling 69:79–79

Chiocci FL, Romagnoli C, Bosman A (2008) Morphologic resilience and depositional processes due to the rapid evolution of the submerged Sciara del Fuoco (Stromboli Island) after the December 2002 submarine slide and tsunami. Geomorphology 100:356–365. https://doi.org/10.1016/j.geomorph.2008.01.008

Dao MH, Xu H, Chan ES, Tkalich P (2013) Modelling of tsunami-like wave run-up, breaking and impact on a vertical wall by SPH method. Natural Hazards and Earth System Sciences 13:3457–3467. https://doi.org/10.5194/nhess-13-3457-2013

Didenkulova II, Pelinovsky EN, Soomere T (2009) Runup characteristics of symmetrical solitary tsunami waves of "unknown" shapes. Pure Appl Geophys 165:2249–2264. https://doi.org/10.1007/s00024-008-0425-6

Enet F, Grilli ST (2007) Experimental study of tsunami generation by three-dimensional rigid underwater landslides. Journal of Waterway, Port, Coastal, and Ocean Engineering 133:442–454

Ezersky A, Tiguercha D, Pelinovsky E (2013) Resonance phenomena at the long wave run-up on the coast. Natural Hazards and Earth System Sciences 13:2745–2752. https://doi.org/10.5194/nhess-13-2745-2013

Fabbri A, Gallignani P, Zitellini N (1981) Geological evolution of the peri-Tyrrhenian sedimentary basins. Tecnoprint, Bologna, pp 101–126

Federici B, Bacino F, Cosso T, Poggi P, Rebaudengo Landò L, Sguerso D (2006) Analisi del rischio tsunami applicata ad un tratto della costa Ligure. Geomatics Workbooks 6:1–19

Ferranti L, Antonioli F, Anzidei M, Monaco C, Stocchi P (2010) The timescale and spatial extent of vertical tectonic motions in Italy: insights from relative sea-level changes studies. Journal of the Virtual Explorer, Electronic Edition. ISSN:1441-8142 ISSN: 1441-8142, 36, paper 23

Flouri ET, Kalligeris N, Alexandrakis G, Kampanis NA, Synolakis CE (2013) Application of a finite difference computational model to the simulation of earthquake generated tsunamis. Applied Numerical Mathematics 67:111–125. https://doi.org/10.1016/j.apnum.2011.06.003

Gasparo Morticelli M, Valenti V, Catalano R, Sulli A, Agate M, Avellone G, Albanese C, Basilone L, Gugliotta C (2015) Deep controls on foreland basin system evolution along the Sicilian fold and thrust belt. Bulletin de la Societé géologique de France, Special Pubbl. 186:273–290

Gedik N, Irtem E, Kabdasli S (2005) Laboratory investigation on tsunami run-up. Ocean Engineering 32(5–6):513–528

Giunta G, Luzio D, Agosta F, Calò M, Di Trapani F, Giorgianni A, Oliveri E, Orioli S, Perniciaro M, Vitale M, Chiodi M, Adelfio G (2009) An integrated approach to investigate the seismotectonics of northern Sicily and southern Tyrrhenian. Tectonophysics 476:13–21. https://doi.org/10.1016/j.tecto.2008.09.031

Glimsdal S, Pedersen GK, Harbitz CB, Løvholt F (2013) Dispersion of tsunamis: does it really matter? Natural Hazards and Earth System Sciences 13:1507–1526. https://doi.org/10.5194/nhess-13-1507-2013

Gjevik B, Pedersen G (1983) Run-up of solitary waves. Journal of Fluid Mechanics 135:283–299

Grilli ST, Watts P (1999) Modelling of waves generated by a moving submerged body. Applications to underwater landslides. Engineering Analysis with Boundary Elements 23:645–656

Grilli ST, Watts P (2005) Tsunami generation by submarine mass failure I: Modeling, experimental validation, and sensitivity analyses. J Waterway Port Coastal Ocean Eng 1316:283–297

Grilli ST, Svendsen IA, Subramanya R (1997) Breaking criterion and characteristics for solitary waves on slopes. Journal of Waterway, Port, Coastal and Ocean Engineering 123(3):102–112

Harbitz CB, Løvholt F, Pedersen G, Masson DG (2006) Mechanisms of tsunami generation by submarine landslides: a short review. Norwegian Journal of Geology 86:255–264

Heinrich P, Piatanesi A, Okal E, Hèbert H (2000) Near-field modeling of the July 17, 1998 tsunami in Papua New Guinea. Geophysical Research Letters 27(19):3037–3040

Ioualalen M, Pelletier B, Watts P, Regnier M (2006) Numerical modeling of the 26th November 1999 Vanuatu tsunami. Journal of Geophysical Research 111:C06030

Kastens K, Mascle J, Auroux C, Bonatti E, Broglia C, Channell J, Curzi P, Emeis KC, Glacon G, Asegawa S, Hieke W, Mascle G, McCoy F, McKenzie J, Mendelson J, Muller C, Rèhault JP, Robertson A, Sartori R, Sprovieri R, Tori M (1988) ODP Leg 107 in the Tyrrhenian Sea: insights into passive margin and back-arc basin evolution. Geological Society of America Bulletin 100:1140–1156

Kriebel DL, Lynett PJ, Cox DT, Petroff CM, Robertson IN, Chock GYK (2017). Energy method for approximating overland tsunami flows. J. Waterway, Port, Coastal, Ocean Eng., 143(5), 1–19

Labbé M, Donnadieu C, Daubord C, Hébert H (2012) Refined numerical modeling of the 1979 tsunami in Nice (French Riviera): comparison with coastal data. J Geophys Res 117:F01008. 17. https://doi.org/10.1029/2011JF001964

Liu P-F, Wu T-R, Raichlen F, Synolakis CE, Borrero JC (2005) Runup and rundown generated by three-dimensional sliding masses. Journal of Fluid Mechanics 536:107–144

Lo Iacono C, Sulli A, Agate M (2014) Submarine canyons of northwestern Sicily (Southern Tyrrhenian Sea): variability in morphology, sedimentary processes and evolution on a tectonically active margin. Deep-Sea Res II Top Stud Oceanogr 104:93–105

Lo Iacono C, Sulli A, Agate M, Lo Presti V, Pepe F, Catalano R (2011) Submarine canyon morphologies in the Gulf of Palermo (Southern Tyrrhenian Sea) and possible implications for geo-hazard. Marine Geophysical Research 32(1):127–138. https://doi.org/10.1007/s11001-011-9118-0

López-Venegas AM, ten Brink US, Geist EL (2008) Submarine landslide as the source for the October 11, 1918 Mona Passage tsunami: observations and modeling. Marine Geology 254:35–46. https://doi.org/10.1016/j.margeo.2008.05.001

Madsen PA, Fuhrman DR (2008) Run-up of tsunamis and long waves in terms of surf-similarity. Coastal Engin. 55:209–223

Mauz B, Buccheri G, Zöller L, Greco A (1997) Middle to upper Pleistocene morphostructural evolution of the NW-coast of Sicily: thermoluminescence dating and palaeontological-stratigraphical evaluations of littoral deposits. Palaeogeography, Palaeoclimatology, Palaeoecology 128:269–285

McAdoo BG, Watts P (2004) Tsunami hazard from submarine landslides on the Oregon continental slope. Marine Geology 203:235–245. https://doi.org/10.1016/S0025-3227(03)00307-4

Neri G, Caccamo D, Cocina O, Montalto A (1996) Geodynamic implications of recent earthquake data in the Southern Tyrrhenian Sea. Tectonophysics 258:233–249

Nicolsky DJ, Suleimani EN, Hansen RA (2010) Numerical modeling of the 1964 Alaska tsunami in western Passage Canal and Whittier, Alaska. Natural Hazards and Earth System Sciences 10:2489–2505. https://doi.org/10.5194/nhess-10-2489-2010

Parsons T, Geist EL, Ryan HF, Lee HJ, Haeussler PJ, Lynett P, Hart PE, Sliter R, Roland E (2014) Source and progression of a submarine landslide and tsunami: the 1964 Great Alaska earthquake at Valdez. J Geophys Res Solid Earth 119:8502–8516. https://doi.org/10.1002/2014JB011514

Pepe F, Sulli A, Bertotti G, Catalano R (2005) Structural highs formation and their relationship to sedimentary basins in the north Sicily

continental margin (southern Tyrrhenian Sea): implication for the Drepano Thrust Front. Tectonophysics 409:1–18

Sulli A (2000) Structural framework and crustal characteristics of the Sardinia Channel Alpine transect in the central Mediterranean. Tectonophysics 324:321–336

Sulli A, Lo Presti V, Gasparo Morticelli M, Antonioli F (2013) Vertical movements in NE Sicily and its offshore: outcome of tectonic uplift during the last 125 ky. Quaternary International 288:168–182. https://doi.org/10.1016/j.quaint.2012.01.021

Synolakis CE (1987) The runup of solitary waves. Journal of Fluid Mechanics 185:523–545

Synolakis CE, Bardet J-P, Borrero JC, Davies HL, Okal EA, Silver EA, Sweet S, Tappin DR (2002) The slump origin of the 1998 Papua New Guinea tsunami. Math Phys Eng Sci 458:763–789

Tappin D R (2017) The generation of tsunamis. Encyclopedia of Maritime and Offshore Engineering. pp. 1–10

Tappin DR, Watts P, Grilli ST (2008) The Papua New Guinea tsunami of 17 July 1998: anatomy of a catastrophic event. Natural Hazards and Earth System Sciences 8:243–266

Tinti S, Manucci A, Pagnoni G, Armigliato A, Zaniboni F (2005) The 30 December 2002 landslide-induced tsunamis in Stromboli: sequence of the events reconstructed from the eyewitness accounts. NHESS 5(6):763–775

Tinti S, Maramai A, Armigliato A, Graziani L, Manucci A, Pagnoni G, Zaniboni F (2006) Observations of physical effects from tsunamis of December 30, 2002 at Stromboli volcano, southern Italy. Bulletin of Volcanology 68:450–461. https://doi.org/10.1007/s00445-005-0021-x

Tinti S, Zaniboni F, Pagnoni G, Manucci A (2008) Stromboli Island (Italy): scenarios of tsunamis generated. Pure Appl Geophys. 165: 2143–2167. https://doi.org/10.1007/s00024-008-0420-y

Trincardi F, Zitellini N (1987) The rifting of the Tyrrhenian Basin. Geo-Marine Letters 7:1–6

Wiegel RL (1955) Laboratory studies of gravity waves generated by the movement of a submerged body. Trans Am Geophys Union 36(5): 759–774

Zhao XL, Wang B, Liu H (2010) Propagation and runup of tsunami waves with Boussinesq model. Proceedings of the 32nd International Conference on Coastal Engineering, Shanghai, pp 1–14